



pubs.acs.org/NanoLett Letter

Fast Magneto-Ionic Switching of Interface Anisotropy Using Yttria-Stabilized Zirconia Gate Oxide

Ki-Young Lee, Sujin Jo, Aik Jun Tan, Mantao Huang, Dongwon Choi, Jung Hoon Park, Ho-Il Ji, Ji-Won Son, Joonyeon Chang, Geoffrey S. D. Beach, and Seonghoon Woo*



Cite This: Nano Lett. 2020, 20, 3435-3441



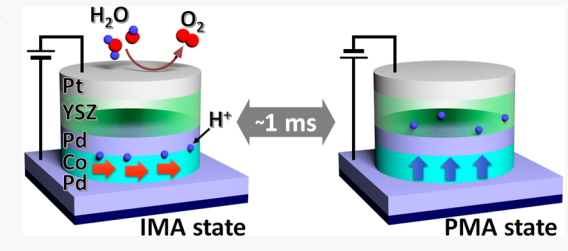
ACCESS

Metrics & More

Article Recommendations

Supporting Information

ABSTRACT: Voltage control of interfacial magnetism has been greatly highlighted in spintronics research for many years, as it might enable ultralow power technologies. Among a few suggested approaches, magnetoionic control of magnetism has demonstrated large modulation of magnetic anisotropy. Moreover, the recent demonstration of magneto-ionic devices using hydrogen ions presented relatively fast magnetization toggle switching, $t_{\rm sw} \sim 100$ ms, at room temperature. However, the operation speed may need to be significantly improved to be used for modern electronic devices. Here, we demonstrate that the speed of proton-induced magnetization toggle



switching largely depends on proton-conducting oxides. We achieve ~ 1 ms reliable (>10³ cycles) switching using yttria-stabilized zirconia (YSZ), which is ~ 100 times faster than the state-of-the-art magneto-ionic devices reported to date at room temperature. Our results suggest that further engineering of the proton-conducting materials could bring substantial improvement that may enable new low-power computing scheme based on magneto-ionics.

KEYWORDS: Voltage controlled magnetic anisotropy, Magneto Ionics, Spintronics, Magnetic heterostructure

lthough nonvolatile spintronics-based devices are seen as candidates to replace conventional CMOS technologies, electrical current-induced magnetization switching is energyintensive,2 which has hindered the implementation of spintronics in low-power applications. For example, although recent developments in spin-transfer-torque magnetoresistive random access memory (STT-MRAM) have reduced the switching energy to ~ 100 fJ/bit, 3,4 the energy consumption is still much higher than that of conventional static-RAM (SRAM), which STT-MRAM is being targeted to replace in some applications.² Voltage-control of magnetic anisotropy,^{5,6} in which a gate voltage applied across a thin oxide layer modulates the magnetization switching energy barrier in an adjacent ferromagnet, has attracted significant attention in recent years, owing to the much reduced switching energies in devices. Although multiple approaches have been demonstrated experimentally, 2,7-16 voltage-controlled ionic motion leading to magnetic anisotropy modulation, known as magneto-ionic control of magnetic anisotropy, 9-16 has yielded high-efficiency anisotropy modulations up to ~ 1 erg cm⁻², 10,11 as required for practical device applications. Early works $^{9-14}$ utilized voltage-induced oxygen ion (O^{2-})

Early works⁹⁻¹⁴ utilized voltage-induced oxygen ion (O²⁻) migration in ferromagnetic heterostructures; however, such a scheme relying on reactive and relatively large oxygen ions suffered from slow switching speed,^{10,17} irreversible oxidation damage,¹³ and high operation temperature.^{10,11} For example, the control of interfacial magnetic anisotropy using O²⁻ ions requires >100 s at room temperature, thereby requiring a high

temperature of >250 °C in order to reduce the switching speed down to ~30 s.¹⁷ Recently, it has been demonstrated that proton (H⁺)-based magneto-ionic devices could offer significantly enhanced device capabilities, such as nondestructive ~100 ms-speed magnetization switching at room temperature (RT), with robust, reversible operation (proton injection and release) for thousands of switching cycles. 15,16 In these devices, solid-state electrochemical water splitting using atmospheric humidity was shown to provide a source of mobile protons that could be driven through a gate oxide to reversibly switch the magnetic anisotropy between perpendicular magnetic anisotropy (PMA) and in-plane magnetic anisotropy (IMA). 15,16 Considering the nanosecond time scale required for modern data storage and computing devices, however, significant improvements still need to be made. One possible approach is to use an optimized proton-conducting oxide in order to improve the speed of the device, since previous studies have only focused on a single material, GdOx, 15,16 which is not generally considered a good proton conductor.

Here, we show that the speed of proton-induced magnetization switching depends largely on the proton conductivity of

Received: January 25, 2020 Revised: April 24, 2020 Published: April 28, 2020





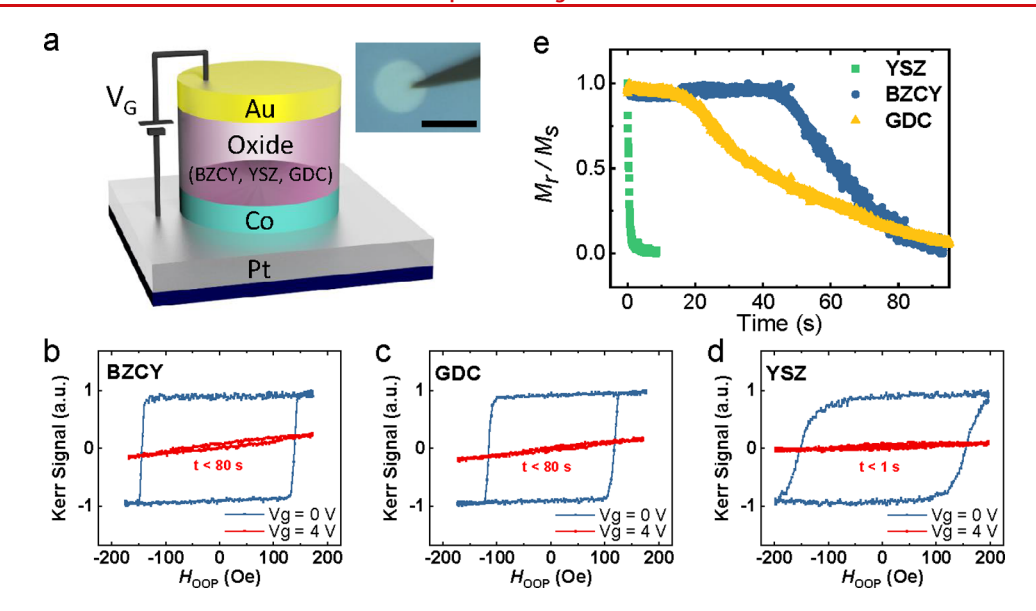


Figure 1. Magneto-ionic switching of ferromagnetic heterostructures with various oxides. (a) Schematic of magnetic heterostructure of Pt(3 nm)/Co(1 nm)/oxides(10 nm)/Au (3 nm) for MOKE measurements. The inset shows an optical micrograph of the probe-landed device. Scale bar, 50 μ m. Out-of-plane hysteresis loops measured in the devices with (b) BZCY, (c) GDC, and (d) YSZ, respectively, under a gate voltage of $V_G = 0$ V (blue line) and $V_G = +4$ V (red line). (e) Out-of-plane magnetization remanence ratio, M_r/M_s , measured by MOKE, where M_r is the remnant magnetization and M_s is the saturation magnetization as a function of gate voltage application time at $V_G = +4$ V, corresponding to BZCY (blue), GDC (yellow), and YSZ (green) gate oxides.

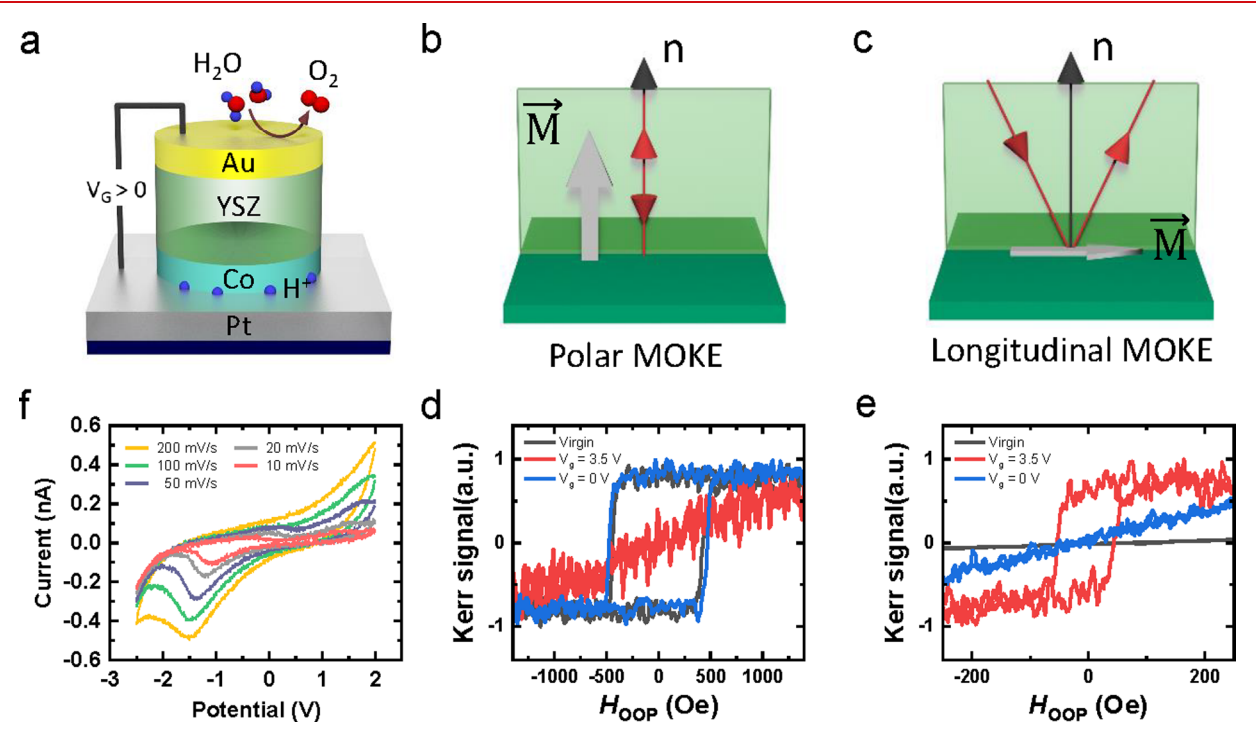


Figure 2. Proton-induced magnetization rotation in the structure using YSZ gate oxide. (a) Schematic of magneto-ionic switching mechanism in a Pt(3 nm)/Co(1 nm)/YSZ(10 nm)/Au (3 nm) structure device. (b, c) Schematics of polar and longitudinal MOKE measurement configurations, respectively. (d, e) Polar MOKE and longitudinal MOKE hysteresis loops in the virgin state (black line), after applying $V_G = +3.5$ V (red line) and after V_G is removed (blue line). (f) Cyclic voltammetry measurement plot at various sweep rates performed in an ambient atmosphere using a Au(10 nm)/YSZ(50 nm)/Pt(3 nm) structure.

the proton-conducting oxide material. By comparing various complex oxides known for their efficient proton conductivity, ¹⁸ namely, gadolinium-doped ceria (GDC), barium cerium yttrium zirconate (BZCY), and yttria-stabilized zirconia (YSZ), we demonstrate fast (~1 ms) and reliable (>10³ cycles) magnetization switching in ultrathin ferromagnetic

heterostructures employing YSZ gate oxides. The observed speeds are two orders of magnitude faster than the state-of-theart device reported to date at RT. Systematic material and thickness studies reveal a path toward optimization of the device structure for efficient electrochemical interface reactions

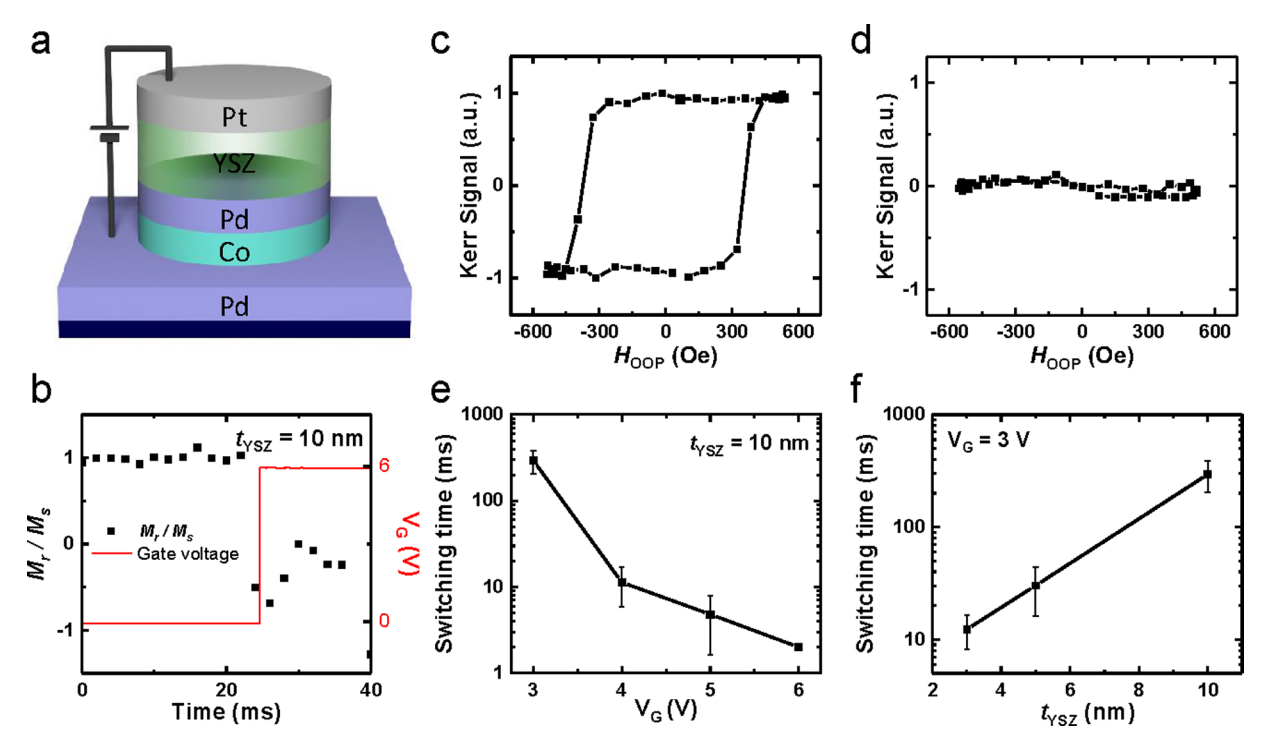


Figure 3. Fast switching of magnetic anisotropy in an engineered structure with YSZ gate oxide. (a) Schematic of device with optimized structure for fast magnetization switching, $Pd(3 \text{ nm})/Pd(1 \text{ nm})/YSZ(t_{YSZ} \text{ nm})/Pt(3 \text{ nm})$, where t_{YSZ} is controlled between 3 and 10 nm. (b) Polar MOKE measurement of the remanence ratio (M_v/M_s) upon gate voltage application, $V_G = +6$ V. Out-of-plane hysteresis loops right (c) before (where $V_G = 0$ V) and (d) after (where $V_G = +6$ V) the gate voltage application. Magnetization switching time, t_{sw} , as a function of (e) gate voltage amplitude, V_G , and (f) YSZ gate oxide thickness, t_{YSZ} , respectively.

and fast ion transport, which may push the switching speed toward levels suitable for data handling device applications.

Proton conducting oxides have been widely studied in the context of solid oxide fuel cells (SOFCs), where high proton mobility at low temperature ($T < 500\,^{\circ}\text{C}$) is required for efficient device implementations. ^{18–21} Among various classes of oxides, enhanced ionic conductivity has been achieved in fluorite-structure-doped ZrO_2 and CeO_2 , such as yttriastabilized ZrO_2^{22} and gadolinium-doped CeO_2^{23} as well as perovskite-structured mixed oxides such as (yittria-doped) $\text{BaCeO}_3\text{-BaZrO}_3$. ²⁴ These oxides are stable under electrochemical reactions (i.e., reduction or oxidation) and present large (small) ionic (electronic) conductivities. These same characteristics make them particularly suitable as proton conductors in proton-based magneto-ionic devices. In this study, we examine magneto-ionic switching in heterostructures employing such protonic oxides as gate electrodes.

Figure 1 summarizes the effect of gate voltage application to Pt(3 nm)/Co(1 nm)/oxide(20 nm)/Au(10 nm) ferromagnetic heterostructures with perpendicular magnetic anisotropy, where GDC, BZCY, and YSZ were used as gate oxides [see the Methods section for device fabrication details]. Figure 1a shows the schematic of the sample structure and an optical micrograph of a 50 μ m-diameter device. A gate voltage of V_G = +4 V was applied to the top Au electrode using a BeCu microprobe while the bottom Pt was grounded. The hysteresis behavior of magnetic heterostructures was characterized by polar magnetic-optic Kerr effect (MOKE) measurements, as shown in Figure 1b—d. Note that all magnetic heterostructures exhibit PMA with similar coercive fields in the as-grown states, implying that PMA may originate from strong interfacial spin—orbit coupling between the Pt and Co layers. Moreover,

prolonged application of positive gate-bias eventually eliminated the PMA in all devices. This can be attributed to protoninduced magnetization rotation to an in-plane state as summarized in Figure 2. This result is consistent with recent observation using GdOx, 15,16 revealing the generality of this mechanism. However, the switching time strongly depends on the type of oxide. Figure 1e plots the variation of out-of-plane remnant magnetization ratio (M_r/M_s) as a function of gate-bias application time. Surprisingly, when YSZ was used as the gate oxide, M_r/M_s approaches zero within a time scale $t_{sw} < 1$ s, which is approximately two orders of magnitude faster than for BZCY and GDC. This result implies fast ionic transport in 20 nm-thick YSZ gate oxide grown at room temperature, which likely originates from enhanced proton conductivity through, e.g., grain boundaries, 22,25 which is also largely material and growth condition dependent.26

To verify the underlying mechanism as proton-induced magnetic anisotropy modulation, we performed simultaneous polar- and longitudinal-MOKE and cyclic voltammetry (CV) measurements as shown in Figure 2. Figure 2a shows the schematic description of proton-induced magnetic anisotropy switching. In this scheme, as was briefly explained in the introduction, upon the application of a positive voltage exceeding ~1.2 V, atmospheric water (humidity) is electrolyzed at the top electrode to produce H⁺ and O₂ gas. The generated protons are transported to the bottom electrode through the oxide via a Grotthuss-type hopping mechanism, T5,20 where their presence modulates interfacial magnetic anisotropy at YSZ/Co and Co/Pt interfaces. Figure 2b-e present out-of-plane and in-plane hysteresis loops for Pt/Co/ YSZ heterostructures, measured by polar and longitudinal MOKE. The MOKE geometry was switched between polar

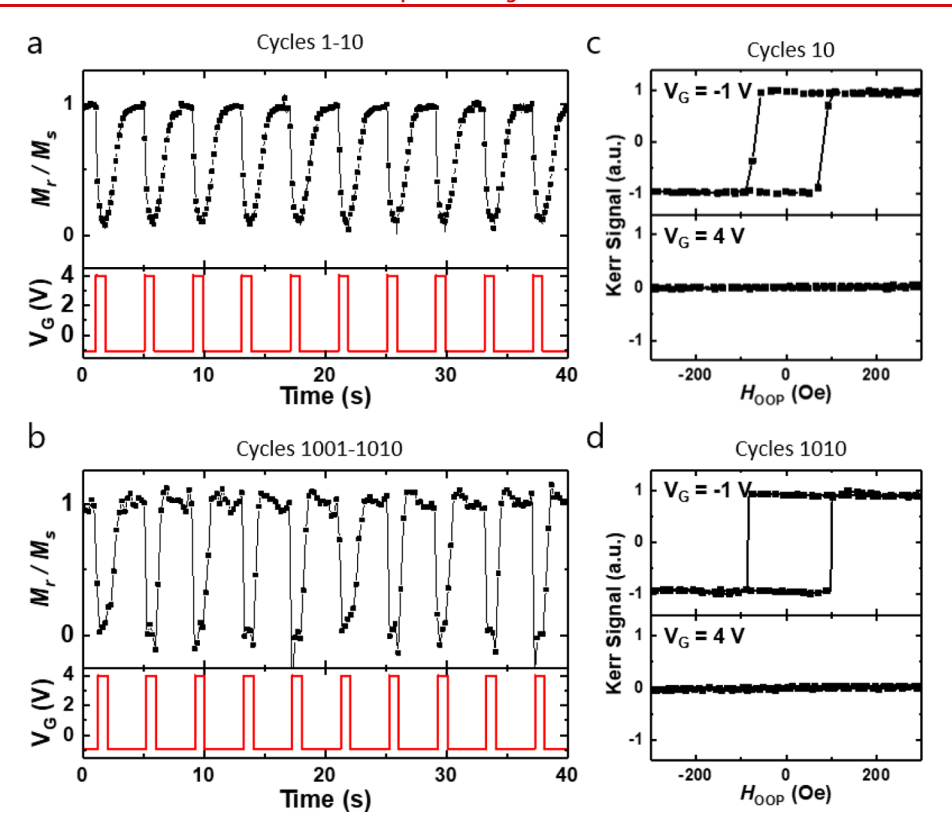


Figure 4. Reliable switching of magnetic anisotropy. The out-of-plane remnant magnetization ratio (M_r/M_s) as a function of voltage cycle for (a) cycles 1–10 and (b) cycles 1001–1010, respectively. Hysteresis loops under gate voltage measured by Polar MOKE for (c) cycle 10 and (d) cycle 1010. Note that $V_G = -1$ V is used here to accelerate the process of in-plane (IP) to out-of-plane (OOP) magnetization transition with limited oxidation of Co.

and longitudinal configurations (Figure 2b, c) to successively probe the out-of-plane and in-plane hysteresis behavior every 10 s. In the virgin state (black line in Figure 2d, e), square and linear loops are measured using polar and longitudinal MOKE, respectively, implying an initial PMA state.

However, upon application of $V_G = +3.5$ V, the magnetization rotates in plane (red line in Figure 2d, e), corresponding to hydrogen accumulation at the YSZ/Co and Co/Pt interfaces. When the gate voltage set to zero (shortcircuiting the top and bottom electrode), PMA spontaneously recovers and remains stable (blue line in Figure 2d, e), as accumulated protons at the interfaces are removed. 15 We then performed CV measurement for a Au(10 nm)/YSZ(50 nm)/ Pt(3 nm) structure at different sweep rates, as shown in Figure 2f. Although cathodic and anodic currents were observed for all sweep rates, the magnitude of the current was governed by the voltage sweep rate, suggesting that the process is mass transport-limited rather than charge-transport limited.²⁷ Therefore, the polarity of gate voltage used for magnetization rotation and the mass transport nature revealed from CV data are consistent with voltage-induced proton pumping inferred from the magnetic measurements heterostructures, as also reported elsewhere.15

Having examined the mechanism and observed that proton-induced magnetization switching can take place in YSZ-based magnetic heterostructures efficiently, we then demonstrate the fast and robust switching of magnetization in further engineered YSZ-based heterostructures. Figure 3a shows the schematic of a Pd(3 nm)/Co(1 nm)/Pd(1 nm)/YSZ($t_{\rm YSZ}$ nm)/Pt(3 nm) structure used for fast switching experiments, where $t_{\rm YSZ}$ is controlled between 3 and 10 nm. Compared to

the previous structures used for Figure 1 and Figure 2, we first substituted Au with Pt for the top electrode, as Pt is known as an excellent catalyst for oxygen evolution reaction (OER).²⁸ This supposition is supported by our direct comparison between Au and Pt on cyclic voltage application experiments, as shown in Figure S1. Moreover, we introduced a thin layer of Pd as a hydrogen loading layer²⁹ between Co and YSZ, where the addition of Pd is expected to protect Co from degradation over many switching cycles [see Figure S2 and Figure S3]. We also replaced the bottom Pt reference electrode with a Pd layer, so that a larger quantity of hydrogen can be absorbed at the Pd/Co interface, inducing more efficient change in interfacial magnetic anisotropy from the Pd/Co interface. Figure 3b plots the change of the out-of-plane remnant magnetization ratio (M_r/M_s) upon $V_G = +6$ V gate voltage application on a $t_{YSZ} = 6$ nm sample, and Figures 3c and 3d plot the measured out-ofplane hysteresis loops right before (Figure 3c) and right after (Figure 3d) the gate voltage application. In this measurement scheme, we sweep the out-of-plane magnetic field and measure M_r/M_s via hysteresis loops measured at a field sweep rate of 500 Hz, corresponding to a time resolution of 2 ms. As shown in Figure 3b-d, upon gate voltage application, the magnetization rotates from PMA to in-plane instantaneously within the time resolution of the current setup. This fast switching in the millisecond regime is two orders of magnitude faster than the state-of-the-art magneto-ionic device reported to date at room temperature, which was recently demonstrated with a GdO_x gate oxide using proton-induced magneto-ionic switch-

Figure 3e plots the effective magnetization switching time, t_{sw} , as a function of gate voltage amplitude at $t_{YSZ} = 10$ nm,

where t_{sw} exponentially decreases from $t_{sw} = 290$ ms ($V_G = +3$ V) to $t_{\rm sw} \sim {\rm sub} - 2~{\rm ms}~(V_{\rm G} = +6~{\rm V})$ as the gate voltage increases. This exponential decrease suggests a mobility-limited switching time, which is expected to scale exponentially with the electric field.³⁰ The electric field can also be varied by controlling the YSZ thickness. As seen in Figure 3f, the switching time varies exponentially with gate oxide thickness, for a fixed gate voltage $V_G = +3$ V, corresponding to a value appropriate for applications. It should be noted that our experiments use a mechanical probe to contact the top electrode, which limits the YSZ thickness to >3 nm to prevent mechanical shorting; such limitations can be eliminated using microfabricated top gate contacts, such that even thinner gate oxides and consequently faster operation can reasonably be expected. From Figure 3f, we estimate that an effective YSZ thickness below 1 nm could bring the operation speed down to the microsecond and even nanosecond regime in the current scheme.

We next examine the endurance of this YSZ-based magnetoionic device with a $t_{YSZ} = 10$ nm device, as summarized in Figure 4. Figure 4a and b present M_r/M_s extracted from polar MOKE hysteresis loop measurements as a function of voltage cycle, for cycles 1-10 and 1001-1010, tracking in-plane/outof-plane transitions as V_G is cycled between +4 V and -1 V. The asymmetric voltage amplitudes are chosen to maintain the high speed of operation at both loading/unloading processes, while minimizing oxidation of Co, which occurs with repeated cycling at higher negative bias. Figure 4c and d show corresponding magnetization hysteresis loops measured by polar MOKE at cycle 10 and cycle 1010, respectively, revealing the robust reliability of YSZ-based heterostructures for >10³ cycles. Moreover, it is noteworthy that the effective switching speed increases with repeated measurements, implying efficient proton paths are established in the YSZ oxide through repeated cycling.

In conclusion, we have shown that magneto-ionic control of magnetic anisotropy can be highly efficient in ferromagnetic heterostructures using an YSZ gate oxide as a solid-oxide proton electrolyte. Using engineered heterostructure consisting of Pd/Co/Pd/YSZ/Pt, we demonstrate ~millisecond magnetization toggle switching between out-of-plane and in-plane magnetization states. The switching speed can further be engineered by controlling the gate oxide thickness or increasing the voltage amplitude to increase the driving electric field. We also demonstrate robust device endurance with 10³ voltage cycles. Together, we believe this work establishes that gate oxide material engineering may be a key pathway for achieving fast and reliable switching in magnetoionic devices, highlighting the significant potential of this approach toward future spintronic applications.

METHODS

Sample Preparation. Ta/(Pt or Pd)/Co/(Pd or not) films were deposited on thermally oxidized Si wafers using a dc-magnetron sputtering at Ar 2 mTorr partial pressure, where the bottom Ta layer serves as a seed layer. Proton conducting oxide (BZCY, GDC, YSZ) layers were deposited by using pulsed laser deposition (PLD) with a KrF excimer laser (λ = 248 nm) and O₂ pressure of ~50 mTorr at room temperature, therefore leading to an amorphous microstructure [see Figure S4 for details]. For gate voltage application, 50- μ m diameter Au or Pt (3 nm) top electrodes were patterned using shadow masks. The bottom continuous metal layer was exposed at the sample edge and was contacted directly for use as counter-

electrode. Cross-sectional transmission electron microscopy (TEM) image of an exemplary Pt/Co/YSZ/Pt heterostructure is shown in Figure S5.

Polar and Longitudinal MOKE Measurement. Polar and longitudinal MOKE measurements were performed using a 660 nm diode laser attenuated to 1 mW. The laser was focused to a spot size of about $\sim 3 \mu m$ diameter. The gate voltage $V_{\rm G}$ was applied using a mechanically compliant BeCu microprobe tip. This probe tip was placed near the edge of the top electrode to avoid overlap with the MOKE laser spot position, and the Ta/Pt or Pd back electrode was grounded using another tungsten microprobe tip. The laser spot was focused on the middle of the electrode. For cyclic voltage application experiments, we obtained the hysteresis loop using polar MOKE measurement, where the gate voltage was applied using a function generator. The M_r/M_s value of each point was acquired from individual out-of-plane hysteresis loops at each measurement recorded at every 2 ms. Note that the time resolution is a limitation of the current measurement setup, and the effective coercivity of the magnetic heterostructure at higher field-sweep frequencies exceeds the maximum available magnetic field amplitude. Moreover, the total number of cycles in voltage switching measurements was limited to ~1,000 cycles, since the mechanical vibration of the system often leads to loss of electrical contact of the BeCu microprobes.

Cyclic Voltammetry Measurement. A Au(10 nm)/YSZ(50 nm)/Pt(3 nm) heterostructure was fabricated for the cyclic voltammetry (CV) measurements. CV measurements were performed using a PARSTAT MC potentiostat (Princeton Applied Research). The top Pt layer and bottom Au layer act as the working electrode and the counter/reference electrode, respectively. The scan rate varied from 10 to 200 mV s⁻¹.

ASSOCIATED CONTENT

Supporting Information

The Supporting Information is available free of charge at https://pubs.acs.org/doi/10.1021/acs.nanolett.0c00340.

Figures S1—S5 as referenced in the main text, including cyclic voltage application experimental data on additional heterostructure devices (Pd/Co/Pd/YSZ/Au, Pd/Co/YSZ/Pt, Pt/Co/YSZ/Au) and structural analysis performed using high-resolution transmission electron microscopy (HRTEM) (PDF)

AUTHOR INFORMATION

Corresponding Authors

Geoffrey S. D. Beach — Department of Materials Science and Engineering, Massachusetts Institute of Technology, Cambridge, Massachusetts 02139, United States; Email: gbeach@mit.edu Seonghoon Woo — Center for Spintronics, Korea Institute of Science and Technology, Seoul 02792, Korea; orcid.org/0000-0001-8879-1203; Email: shwoo@ibm.com

Authors

Ki-Young Lee — Center for Spintronics, Korea Institute of Science and Technology, Seoul 02792, Korea; ⊚ orcid.org/ 0000-0002-9327-2026

Sujin Jo – Center for Spintronics, Korea Institute of Science and Technology, Seoul 02792, Korea

- Aik Jun Tan Department of Materials Science and Engineering, Massachusetts Institute of Technology, Cambridge, Massachusetts 02139, United States
- Mantao Huang Department of Materials Science and Engineering, Massachusetts Institute of Technology, Cambridge, Massachusetts 02139, United States; orcid.org/0000-0002-2076-5321
- **Dongwon Choi** Center for Spintronics, Korea Institute of Science and Technology, Seoul 02792, Korea
- Jung Hoon Park Center for Energy Materials Research, Korea Institute of Science and Technology, Seoul 02792, Korea
- Ho-Il Ji Center for Energy Materials Research, Korea Institute of Science and Technology, Seoul 02792, Korea; Nanomaterials Science and Engineering, Korea University of Science and Technology (UST) KIST Campus, Seoul 02792, Korea; orcid.org/0000-0002-6194-991X
- Ji-Won Son Center for Energy Materials Research, Korea Institute of Science and Technology, Seoul 02792, Korea; Graduate School of Energy and Environment (KU-KIST GREEN SCHOOL), Korea University, Seoul 02841, Korea; orcid.org/0000-0002-5310-0633
- Joonyeon Chang Center for Spintronics, Korea Institute of Science and Technology, Seoul 02792, Korea; Department of Materials Science & Engineering, Yonsei University, Seoul 03722, Korea

Complete contact information is available at: https://pubs.acs.org/10.1021/acs.nanolett.0c00340

Author Contributions

^OThese authors contributed equally to this work.

Author Contributions

S.W. and G.S.D.B. planned and supervised the project. S.J. and D.C. fabricated magneto-ionic devices using oxide materials grown by J.H.P., H.-I.J., and J.-W.S.. K.-Y.L. and S.J. performed gating experiments with the support from A.J.T., M.H., and J.C., K.-Y.L., and S.W. drafted the manuscript, and G.S.D.B. revised it with the help from all authors.

Notes

The authors declare no competing financial interest.

ACKNOWLEDGMENTS

This work was partially supported by the KIST Institutional Program (2E29410, 2E30220), the National Research Council of Science and Technology (NST) grant (CAP-16-01-KIST) by the Korea government (MSIP). This work was also partially supported by National Science Foundation (NSF) through the MIT Materials Research Science and Engineering Center (MRSEC) under award number DMR-1419807, and through NSF award number ECCS-1808828. J.C. acknowledges the support of Yonsei-KIST Convergence Research Institute. S.W. acknowledges management support from Guohan Hu and Daniel Worledge at IBM Research.

REFERENCES

- (1) Wolf, S. A.; Awschalom, D. D.; Buhrman, R. A.; Daughton, J. M.; von Molnár, S.; Roukes, M. L.; Chtchelkanova, A. Y.; Treger, D. M. Spintronics: A Spin-Based Electronics Vision for the Future. *Science* **2001**, *294*, 1488–1495.
- (2) Nozaki, T.; Yamamoto, T.; Miwa, S.; Tsujikawa, M.; Shirai, M.; Yuasa, S.; Suzuki, Y. Recent Progress in the Voltage-Controlled Magnetic Anisotropy Effect and the Challenges Faced in Developing Voltage-Torque MRAM. *Micromachines* **2019**, *10*, 327.

- (3) Ando, K.; Fujita, S.; Ito, J.; Yuasa, S.; Suzuki, Y.; Nakatani, Y.; Miyazaki, T.; Yoda, H. Spin-Transfer Torque Magnetoresistive Random-Access Memory Technologies for Normally off Computing (Invited). J. Appl. Phys. 2014, 115, 172607.
- (4) Yuasa, S.; Hono, K.; Hu, G.; Worledge, D. C. Materials for Spin-Transfer-Torque Magnetoresistive Random-Access Memory. *MRS Bull.* **2018**, 43, 352–357.
- (5) Amiri, P. K.; Wang, K. L. Voltage-Controlled Magnetic Anisotropy in Spintronic Devices. SPIN 2012, 02, 1240002.
- (6) Matsukura, F.; Tokura, Y.; Ohno, H. Control of Magnetism by Electric Fields. *Nat. Nanotechnol.* **2015**, *10*, 209–220.
- (7) Maruyama, T.; Shiota, Y.; Nozaki, T.; Ohta, K.; Toda, N.; Mizuguchi, M.; Tulapurkar, A. A.; Shinjo, T.; Shiraishi, M.; Mizukami, S.; Ando, Y.; Suzuki, Y. Large Voltage-Induced Magnetic Anisotropy Change in a Few Atomic Layers of Iron. *Nat. Nanotechnol.* **2009**, *4*, 158–161
- (8) Shiota, Y.; Maruyama, T.; Nozaki, T.; Shinjo, T.; Shiraishi, M.; Suzuki, Y. Voltage-Assisted Magnetization Switching in Ultrathin Fe80Co20 Alloy Layers. *Appl. Phys. Express* **2009**, *2*, 063001.
- (9) Bauer, U.; Emori, S.; Beach, G. S. D. Voltage-Controlled Domain Wall Traps in Ferromagnetic Nanowires. *Nat. Nanotechnol.* **2013**, *8*, 411–416.
- (10) Bauer, U.; Yao, L.; Tan, A. J.; Agrawal, P.; Emori, S.; Tuller, H. L.; van Dijken, S.; Beach, G. S. D. Magneto-Ionic Control of Interfacial Magnetism. *Nat. Mater.* **2015**, *14*, 174–181.
- (11) Bi, C.; Liu, Y.; Newhouse-Illige, T.; Xu, M.; Rosales, M.; Freeland, J. W.; Mryasov, O.; Zhang, S.; te Velthuis, S. G. E.; Wang, W. G. Reversible Control of Co Magnetism by Voltage-Induced Oxidation. *Phys. Rev. Lett.* **2014**, *113*, 267202.
- (12) Li, H.-B.; Lu, N.; Zhang, Q.; Wang, Y.; Feng, D.; Chen, T.; Yang, S.; Duan, Z.; Li, Z.; Shi, Y.; Wang, W.; Wang, W.-H.; Jin, K.; Liu, H.; Ma, J.; Gu, L.; Nan, C.; Yu, P. Electric-Field Control of Ferromagnetism through Oxygen Ion Gating. *Nat. Commun.* **2017**, 8, 1–7.
- (13) Gilbert, D. A.; Grutter, A. J.; Arenholz, E.; Liu, K.; Kirby, B. J.; Borchers, J. A.; Maranville, B. B. Structural and Magnetic Depth Profiles of Magneto-Ionic Heterostructures beyond the Interface Limit. *Nat. Commun.* **2016**, *7*, 12264.
- (14) Grutter, A. J.; Gilbert, D. A.; Alaan, U. S.; Arenholz, E.; Maranville, B. B.; Borchers, J. A.; Suzuki, Y.; Liu, K.; Kirby, B. J. Reversible Control of Magnetism in La0.67Sr0.33MnO3 through Chemically-Induced Oxygen Migration. *Appl. Phys. Lett.* **2016**, 108, 082405
- (15) Tan, A. J.; Huang, M.; Avci, C. O.; Büttner, F.; Mann, M.; Hu, W.; Mazzoli, C.; Wilkins, S.; Tuller, H. L.; Beach, G. S. D. Magneto-Ionic Control of Magnetism Using a Solid-State Proton Pump. *Nat. Mater.* **2019**, *18*, 35–41.
- (16) Tan, A. J.; Huang, M.; Sheffels, S.; Büttner, F.; Kim, S.; Hunt, A. H.; Waluyo, I.; Tuller, H. L.; Beach, G. S. D. Hydration of Gadolinium Oxide (GdOx) and Its Effect on Voltage-Induced Co Oxidation in a Pt/Co/GdOx/ Au Heterostructure. *Phys. Rev. Materials* **2019**, *3*, 064408.
- (17) Bi, C.; Liu, Y.; Newhouse-Illige, T.; Xu, M.; Rosales, M.; Freeland, J. W.; Mryasov, O.; Zhang, S.; te Velthuis, S. G. E.; Wang, W. G. Reversible Control of Co Magnetism by Voltage-Induced Oxidation. *Phys. Rev. Lett.* **2014**, *113*, 267202.
- (18) Kreuer, K. D. Proton-Conducting Oxides. *Annu. Rev. Mater. Res.* **2003**, *33*, *333*–359.
- (19) Iwahara, H. Proton Conducting Ceramics and Their Applications. *Solid State Ionics* **1996**, 86–88, 9–15.
- (20) Kreuer, K.-D. Proton Conductivity: Materials and Applications. *Chem. Mater.* **1996**, *8*, 610–641.
- (21) Steele, B. C. H.; Heinzel, A. Materials for Fuel-Cell Technologies. *Nature* **2001**, *414*, 345–352.
- (22) Avila-Paredes, H. J.; Chen, C.-T.; Wang, S.; De Souza, R. A.; Martin, M.; Munir, Z.; Kim, S. Grain Boundaries in Dense Nanocrystalline Ceria Ceramics: Exclusive Pathways for Proton Conduction at Room Temperature. *J. Mater. Chem.* **2010**, 20, 10110–10112.

- (23) Shirpour, M.; Gregori, G.; Merkle, R.; Maier, J. On the Proton Conductivity in Pure and Gadolinium Doped Nanocrystalline Cerium Oxide. *Phys. Chem. Chem. Phys.* **2011**, *13* (3), 937–940.
- (24) Yang, L.; Zuo, C.; Wang, S.; Cheng, Z.; Liu, M. A Novel Composite Cathode for Low-Temperature SOFCs Based on Oxide Proton Conductors. *Adv. Mater.* **2008**, *20*, 3280–3283.
- (25) Maglia, F.; Tredici, I. G.; Anselmi-Tamburini, U. Densification and Properties of Bulk Nanocrystalline Functional Ceramics with Grain Size below 50nm. *J. Eur. Ceram. Soc.* **2013**, *33*, 1045–1066.
- (26) De Souza, R. A.; Munir, Z. A.; Kim, S.; Martin, M. Defect Chemistry of Grain Boundaries in Proton-Conducting Solid Oxides. *Solid State Ionics* **2011**, *196*, 1–8.
- (27) Bard, A. J.; Faulkner, L. R. Electrochemical Methods: Fundamentals and Applications, 2nd ed.; John Wiley & Sons, Inc.: New York, 2000.
- (28) Trasatti, S. Work Function, Electronegativity, and Electrochemical Behaviour of Metals: III. Electrolytic Hydrogen Evolution in Acid Solutions. *J. Electroanal. Chem. Interfacial Electrochem.* **1972**, 39, 163–184.
- (29) Adams, B. D.; Chen, A. The Role of Palladium in a Hydrogen Economy. *Mater. Today* **2011**, *14*, 282–289.
- (30) Yang, J. J.; Strukov, D. B.; Stewart, D. R. Memristive Devices for Computing. *Nat. Nanotechnol.* **2013**, *8*, 13–24.